Research Article

Cancer Prevention Research

A Novel Preclinical Method to Quantitatively Evaluate Early-Stage Metastatic Events at the Murine Blood–Brain Barrier

Chris E. Adkins[1,2], Mohamed I. Nounou[2,3], Rajendar K. Mittapalli[2], Tori B. Terrell-Hall[1,2], Afroz S. Mohammad[1,2], Rajaganapathi Jagannathan[1], and Paul R. Lockman[1,2]

Abstract

The observation that approximately 15% of women with disseminated breast cancer will develop symptomatic brain metastases combined with treatment guidelines discouraging single-agent chemotherapeutic strategies facilitates the desire for novel strategies aimed at outright brain metastasis prevention. Effective and robust preclinical methods to evaluate early-stage metastatic processes, brain metastases burden, and overall mean survival are lacking. Here, we develop a novel method to quantitate early metastatic events (arresting and extravasation) in addition to traditional end time-point parameters such as tumor burden and survival in an experimental mouse model of brain metastases of breast cancer. Using this method, a reduced number of viable brain-seeking metastatic cells (from 3,331 ± 263 cells/brain to 1,079 ± 495 cells/brain) were arrested in brain one week postinjection after TGFβ knockdown. Treatment with a TGFβ receptor inhibitor, galunisertib, reduced the number of arrested cells in brain to 808 ± 82 cells/brain. Furthermore, we observed a reduction in the percentage of extravasated cells (from 63% to 30%) compared with cells remaining intralumenal when TGFβ is knocked down or inhibited with galunisertib (40%). The observed reduction of extravasated metastatic cells in brain translated to smaller and fewer brain metastases and resulted in prolonged mean survival (from 36 days to 62 days). This method opens up potentially new avenues of metastases prevention research by providing critical data important to early brain metastasis of breast cancer events. *Cancer Prev Res; 8(1); 68–76. ©2014 AACR.*

Introduction

The annual occurrence of brain metastases arising from primary breast cancer continues to accelerate (1, 2) while therapeutic interventions and our knowledge of metastatic process have not improved significantly over the last few decades. Currently, women diagnosed with multiple brain metastases are primarily left with palliative treatment as clinical interventions involving radiation, surgery, and chemotherapy offer little benefit at this stage; unfortunately, only about 1 in 5 women are expected to survive greater than 12 months after diagnosis of brain metastases (3, 4).

Conventional chemotherapy fails to differentiate between primary breast tumors and their distant central nervous system (CNS) metastases, which may contribute to a patient's rapid decline in quality of life and eventual death (5). Moreover, clinical trials aimed at treating brain metastases using traditional breast cancer drugs have produced little success (6–9). The poor outcome of chemotherapy likely develops from the failure of sufficient drug to penetrate the blood–brain barrier (BBB) and the blood–tumor barrier (BTB), which establishes a protective environment for metastatic growth within the brain.

Given that the current strategies against brain metastases have limitations, there are two developing alternative options that show promise. First, the development of BBB penetrating antineoplastic drugs and, second, therapeutic approaches aimed at the outright prevention of the development of brain metastases of breast cancer. The approach aimed at enhancing the BBB penetration of chemotherapeutic agents is not a new concept. Lipinski's Rule of 5 describes physiochemical factors which predict that a molecule's permeability has been used to design drugs to increase CNS penetration (10). However, anticancer drugs such as chlorambucil and lapatinib, which have greater permeability than traditional chemotherapeutic drugs, also have a higher volume of distribution throughout the rest of the body, which results in an overall decreased total brain accumulation of the drug (11–13).

The lack of accurate and representative *in vivo* preclinical models that are available to study the metastasis pathway is limited. A number of well-defined *in vitro* models such as the migration and invasion assays attempt to characterize metastatic potential (14), but each fail to mimic the complete metastatic cascade *in vivo* (15) due to deficiencies of *in vitro* environments to replicate the structural and physiologic characteristics present *in vivo* (16). Although there are currently reliable *in vivo* models that study metastases growth and development (17–19), their endpoints are typically limited to the number of metastases that developed, metastases size, and mean overall survival. These endpoint parameters do not provide specific insight about when metastatic cells cross the BBB via extravasation, how efficient each of the steps of metastasis are, which steps of metastasis are affected

[1]Department of Basic Pharmaceutical Sciences, Health Sciences Center, School of Pharmacy, West Virginia University, Morgantown, West Virginia. [2]Department of Pharmaceutical Sciences, Texas Tech University Health Sciences Center, School of Pharmacy, Amarillo, Texas. [3]Department of Pharmaceutics, School of Pharmacy, Alexandria University, Alexandria, Egypt.

Corresponding Author: Paul R. Lockman, Department of Basic Pharmaceutical Sciences, West Virginia University Health Sciences Center, 1 Medical Center Drive, Morgantown, WV 26506-9050. Phone: 304-293-0944; Fax: 304-293-0944; E-mail: prlockman@hsc.wvu.edu

doi: 10.1158/1940-6207.CAPR-14-0225

by preventative chemotherapeutics, and whether these models are clinically appropriate (20).

On the basis of the limitations of the current assays to evaluate potential therapies aimed at preventing metastasis, herein we developed a novel *in vivo* method to specifically study seeding and extravasation, two steps critical to the metastatic pathway. This method is relatively quick, robust, and allows for the ability to correlate these early-stage metastatic events to preclinical outcomes.

Using this method, we have observed that inhibition of the TGFβ signaling pathway (a mechanism involved in brain-specific metastasis; ref. 17) resulted in fewer metastatic MDA-MB-231Br cells seeding brain and fewer cells that could extravasate across the BBB into brain tissue. This reduction in brain vascular extravasation resulted in smaller and fewer brain metastases in addition to increased overall survival. Together, these data demonstrate the potential of this method to be used as a robust and translatable assay to simultaneously study both the metastatic pathway and/or pharmacologic targets aiming to enhance the prevention of metastasis.

Materials and Methods

Mice

Female athymic Nu/Nu mice (24–30 g) were purchased from Charles River Laboratories and were used as the experimental metastases platform in this study. All animals were 6 to 8 weeks of age at the initiation of the metastasis model. Animals were housed in a barrier facility. All studies were approved by the Animal Care and Use Committee at Texas Tech University Health Sciences Center (Amarillo, TX), and conducted in accordance with the 1996 NIH Guide for the Care and Use of Laboratory Animals.

Human breast cancer cell lines

A brain-seeking variant of the triple-negative human breast cancer cell line MDA-MB-231 (21) stably transfected with *firefly* luciferase (referred to as 231-Br) was used for both the metastasis model as well as the parent cell for the TGFβ knockdown experiment.

Knockdown expression of hTGF-β2 in BrLuc brain-seeking breast cancer cell line (MDA-MB-231Br) mediated by shRNA

shRNA specific for the human *TGFβ1* and *TGFβ2* gene was acquired from the Open Biosystems. Clone RHS4430-99365286 was chosen as the target of the human *TGFβ2* transcript. The target sequence consisted of: TGCTGTTGACAGTGAGCGACCACATCTCCTGCTAATGTTATAGTGAAGCCACAGATGTATAACATTAGCAGGAGATGTGGGTGCCTACTGCCTCGGA. The h*TGFβ*-specific shRNA was cloned in the pGIPZ lentiviral expression vector (Open Biosystems). The h*TGFβ*-specific shRNA was cotransfected with five lentiviral packaging plasmids, pTLA1-Pak, pTLA1-Enz, pTLA1-Env, pTLA1-Rev, and pTLA1-TOFF, into HEK-293T cells using calcium phosphate as the chemical transfecting agent (Open Biosystems) to produce shRNA carrying lentivirus particles (22, 23). Culture supernatants were collected at 48 hours after transfection and filtered through 0.45μm membranes to generate cell-free virus supernatant. Transfected HEK-293T cells were selected and maintained in puromycin to produce a high yield transfection (0.75 μg/mL). BrLuc cells were transduced by the resulting viral particles; positive clones were selected and maintained in puromycin (1 μg/mL). MTT assay was used to determine the minimal puromycin concentration that can kill nontransfected or transduced cells without affecting the cell viability of the transfected or transduced cells in both HEK-293T and BrLuc cell lines. The enhanced GFP was the primary reporter gene in the shRNA plasmid, which was used to detect expression efficiency across generations on a daily basis using an inverted epifluorescence microscope (Olympus IX81; Olympus). All cells were maintained in DMEM supplemented with 10% FBS, 1% nonessential amino acids, 1% sodium pyruvate, and 2% L-glutamine. All cultures used were between 1 and 10 passages and maintained at 37°C with 5% CO_2.

For all *in vivo* studies, cells were detached from the culture dish and collected during the logarithmic growth stage using 0.05% trypsin (w/v). Cell detachment occurred within 2 minutes by gently rocking the flask; immediately following detachment, DMEM containing serum was supplemented to neutralize the trypsin reaction. Cells were then incubated with QTracker quantum dots (Life Technologies) according to the manufacturer's protocol. Cells were pelleted via centrifugation and resuspended in 4°C sterile Ca^{2+}-free and Mg^{2+}-free PBS. After three washing cycles with sterile PBS, cells were resuspended in 4°C serum-free DMEM and diluted to a concentration of 1.75×10^6 cells/mL. Suspensions consisting of viable dispersed cells (no clumps) were used for injections. Cell suspensions were kept on ice until ready for injection.

Metastasis seeding and extravasation

Mice were randomly divided into three groups ($n = 3$–5 for each group): 231Br-Luc (control), 231Br-Luc (galunisertib treated), and 231Br-Luc-TGFβ-KD. Mice were anesthetized under 2% isoflurane and inoculated with 1.75×10^5 human breast cancer cells (231Br-Luc or 231Br-Luc-TGFβ-KD) in the left cardiac ventricle with the aid of a stereotaxic device (Stoelting Co.). For the galunisertib group (LY2157299, purchased from Axon Medchem), mice were orally dosed twice a day (75 mg/kg) starting 24 hours before intracardiac injection of metastatic cells and continued until sacrifice on day 7. Mice that did not demonstrate successful intracardiac injection 1 or 3 hours postinjection, as detected by bioluminescence imaging (BLI), were removed from the study. One week after intracardiac injection, all animals were anesthetized with ketamine and xylazine (100 mg/kg and 8 mg/kg, respectively) and sacrificed. The brain was rapidly removed and flash frozen in isopentane (−65°C) and then stored at −20°C.

Bioluminescent imaging

Mice were injected with D-luciferin potassium salt (150 mg/kg; PerkinElmer) dissolved in sterile 1× PBS via intraperitoneal injection and then anesthetized under 2% isoflurane. Fifteen minutes after intraperitoneal injection of D-luciferin, darkfield images of mice were acquired with an IVIS Lumineer XV (PerkinElmer) to detect bioluminescence. Animals were imaged 1, 3, 6, 9, 12, 24, 48, 72, 96, 120, 144, and 168 hours postintracardiac injection. Regions of interest were drawn according to the circumference of the cranium and all data were reported as radiance (photons/second/cm^2/sr). Statistical analysis was done using one-way ANOVA with Tukey's multiple comparison.

Tissue analysis and staining

Tissue slicing. Brain slices (20 μm thick) were acquired with a cryotome (Leica CM3050S; Leica Microsystems) and transferred

to charged microscope slides. Fluorescence images of brain slices were acquired using a stereomicroscope (Olympus MVX10; Olympus) equipped with a 1.14NA 2× objective and a camera capable of capturing near infrared light (QImaging) using a custom built quantum dot NIR 800 filter (Chroma Technologies) to detect quantum dots. Brain slices were fixed in 4% paraformaldehyde (PFA) and immunofluorescence staining was performed to detect CD-31. A digital image analysis software (SlideBook 5.0; Intelligent Imaging Innovations Inc.) was used to locate fluorescent metastatic cells relative to vessels (CD-31).

Cresyl violet staining

Tissue sections were processed as described above and subsequently fixed using 4% PFA followed by a rinse in PBS for 10 minutes. Staining was performed using 0.1% cresyl violet acetate (Sigma-Aldrich; 15 minutes) followed by rinsing in H_20. Sections were cleared in 70% ethanol (15 seconds), 95% ethanol (30 seconds), and 100% ethanol (30 seconds), respectively. Brightfield microscopic images were obtained with a 2× objective on an inverted microscope (Olympus IX81) equipped with a color camera (Olympus DP71).

Immunofluorescence

Tissues were rehydrated in PBS and then fixed in cold 4% PFA for CD31 (BD Pharmingen). After three washes in PBS (5 minutes), sections were blocked with 10% goat serum and 0.2% Triton-X 100 (1 hour). Primary antibodies were added, followed by overnight incubation at 4°C. After washing, secondary antibodies and DAPI (1 mg/mL) were added and allowed to incubate for 1 hour. Slides were washed, fluorescence mounting medium (DAKO) was added, and coverslips were applied. For qualitative analysis of fluorescent signal, metastatic cells and/or vasculature were identified with QDot NIR 800 signal and CD31 labeling, respectively.

Tumor burden and size study

Two groups of mice were inoculated with either 231Br-Luc ($n = 12$) or 231Br-Luc-TGFβ-KD ($n = 12$) cells (1.75×10^5) via intracardiac injection. Bioluminescence imaging was completed 3 hours postinjection to confirm successful intracardiac injection. Only animals with successful intracardiac injections were allowed to participate in the study. Animals were randomly sacrificed ($n = 4$) at predetermined times (days 21, 28, and 35). The brains were removed rapidly and flash frozen in isopentane (−65°C) before tissue sectioning. Each brain was sectioned and stained with cresyl violet. Tumors were counted and the size determined using brightfield microscopy. Statistical analysis was done using the Mann–Whitney test because too few tumors were detected on day 21 for each group.

Survival study

Animals were inoculated with 231Br-Luc ($n = 22$) or 231Br-Luc-TGFβ-KD ($n = 13$) cells (1.75×10^5) via intracardiac injection. Bioluminescence was performed on the same day to confirm successful intracardiac injection. Only animals with successful intracardiac injections were allowed to participate in the survival analysis. Once neurologic symptoms (e.g., weight loss, lethargy, paraparesis, immobile, etc.) became significant, animals were removed from the study and euthanized. Statistics were calculated using the Gehan–Breslow–Wilcoxon test.

Results

A brain-seeking human breast adenocarcinoma cell line introduced into immune-deficient mice produced brain-specific metastases (Fig. 1). To determine where MDA-MB-231Br-Luc tumor cells distribute after intracardiac injection, BLI imaging was performed at various time points after injection. Within 1-hour postintracardiac injection, a broad BLI signal ($1.02\times10^5 \pm 0.11$ photons/second/cm^2/sr; $n = 4$) was detected in brain as well as peripheral tissue such as kidney ($3.3\times10^4 \pm 0.9$ photons/second/cm^2/sr; Fig. 1A). To determine whether the injected metastatic cells remain localized and viable specifically in brain and not peripheral tissues, we tracked BLI signal in brain and peripheral tissue (kidney) up to 5 days postintracardiac injection. Brain BLI signal remained stable for 48 hours (1 hour: $1.02\times10^5 \pm 0.11$ photons/second/cm^2/sr; 24 hours: $8.8\times10^4 \pm 2.0$ photons/second/cm^2/sr; $n = 4$; $P > 0.05$; Student t test), whereas the BLI from kidney rapidly declined (1 hour: $3.3\times10^4 \pm 0.9$ photons/second/cm^2/sr; 24 hours: $1.4\times10^3 \pm 0.9$ photons/second/cm^2/sr; $n = 4$; $P > 0.05$; Student t test; a ∼96% reduction) from its initial value (Fig. 1B). The BLI signal in brain began to decrease after 48 hours ($4.44\times10^5 \pm 0.89$ photons/second/cm^2/sr) and became undetectable 5 days ($4.62\times10^4 \pm 0.85$ photons/second/cm^2/sr) after injection (Fig. 2C).

Metastases were allowed to grow for 4 to 5 weeks to determine when BLI signal from growing metastases would return. BLI from growing metastases returned (Fig. 1C) as early as 3 weeks after intracardiac injection and continued to increase through week five (data not shown). The pattern of returning BLI signal was not broad as seen during the first 24 hours after intracardiac injection; instead, BLI signal was seen in more focalized regions but remained confined within the cranium of most animals (Fig. 1C). Mice exhibiting pathologic and/or neurologic symptoms in addition to BLI signal from brain were euthanized when

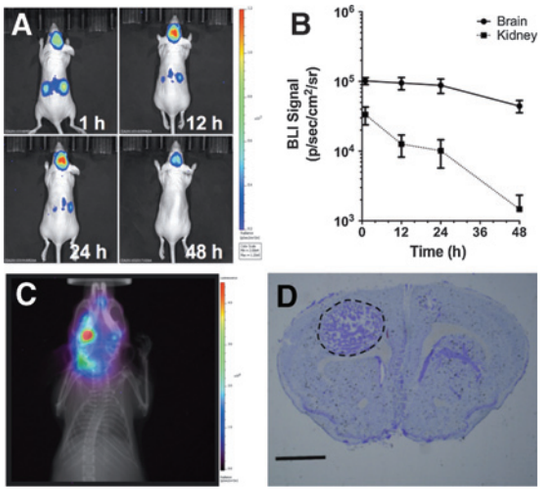

Figure 1.
Brain-seeking MDA-MD-231 specifically metastasizes to brain. Metastatic cells arrest in brain after intracardiac injection and BLI signal remains relatively unchanged during the first 48 hours postinjection (A). BLI is detected both in brain and kidney after intracardiac injection; cells arresting in brain remain viable for 48 hours, whereas cells associated with the kidneys decline rapidly (B). Metastatic 231-Br cells injected intracardially go on to produce large metastasis and are detected by BLI (C). The metastases detected by BLI are confirmed by histologic analysis (D); scale bar = 1 mm.

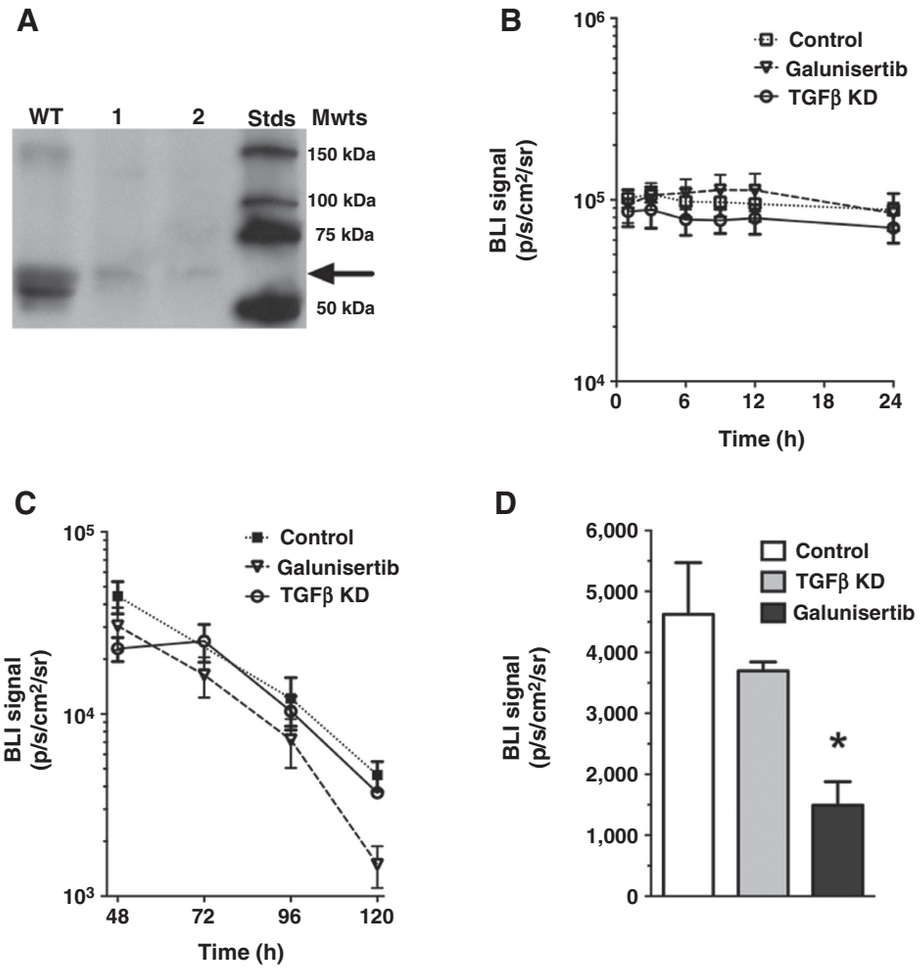

Figure 2.
BLI of metastatic cells is reduced after TGFβ expression knockdown or receptor inhibition. Knockdown of TGFβ in 231-Br observed by Western blot analysis (WT, wild type; lane 1 and 2 show subsequent passages of 231-Br-TGFβ knockdown; A). Normal 231-Br, 231-Br-TGFβ-KD, and galunisertib-treated groups show similar BLI signal during the first 24 hours after intracardiac injection (B), but after 48 hours postintracardiac injection, there is a rapid decline in the BLI signal for each group (C). BLI signal in 231-Br-TGFβ-KD and galunisertib groups reduced by approximately 20% and 68%, respectfully, compared with wild-type 231-Br BLI (D). Each group consists of $n = 3$–5 animals.
*, $P < 0.05$.

neurologic symptoms developed. Histologic analysis of brain tissue confirmed the presence of metastases (Fig. 1D).

To determine the effect of TGFβ signaling on metastatic potential, we administered an orally active TGFβ type I and II receptor inhibitor (galunisertib) or, in a separate group, we knocked down TGFβ expression in 231Br-Luc cells (231Br-Luc-TGFβ-KD) and injected these cells into Nu/Nu mice. TGFβ knockdown was confirmed in two subsequent MDA-MB-231Br-Luc passages with Western blotting (Fig. 2A). TGFβ knockdown and wild-type 231Br-Luc cells (for control and galunisertib groups) were administered via intracardiac injection to female Nu/Nu mice as before. BLI signal for mice injected with 231Br-Luc-TGFβ-KD cells were similar ($P > 0.05$) in intensity ($8.6\times10^4 \pm 1.5$ photons/second/cm^2/sr) and distribution to mice injected with normal 231Br-Luc cells ($8.9\times10^4 \pm 2.0$ photons/second/cm^2/sr) during the first 24 hours (Fig. 2B). The BLI within the first 24 hours in the galunisertib group was also similar in intensity ($8.5\times10^4 \pm 1.2$ photons/second/cm^2/sr) and distribution to the control wild-type 231Br-Luc group. Bioluminescence intensities from galunisertib, TGFβ knockdown, and wild-type 231Br-Luc group began to decrease sharply after 48 hours with 95% of the galunisertib group, approximately 90% of the wild-type 231Br-Luc, and approximately 84% of the TGFβ knockdown cell signal reduced between 48 hours and 120 hours postinjection (Fig. 2C). The BLI intensity in the galunisertib group 5 days postinjection had significantly ($P < 0.05$) lower signal (1,493 ± 385 photons/second/cm^2/sr) than wild-type 231Br-Luc control group (4,622 ± 850 photons/second/cm^2/sr); however, BLI signal observed in the TGFβ knockdown group (3695 ± 148 p/second/cm^2/sr) 5 days after intracardiac injection revealed a 21% less (but not significant; $P > 0.05$) BLI signal compared with the 231Br-Luc control group (Fig. 2D).

We then determined whether a reduction in BLI signal represents a reduction in tumor cells within brain and or brain vasculature. We labeled each group of cells with fluorescence quantum dots before intracardiac injection (Fig. 3A) to determined whether TGFβ knockdown or receptor inhibition using galunisertib reduced tumor cell extravasation from the vessel lumen and subsequent entry into the perivascular space or brain parenchyma using immunofluorescence staining of brain microvessels (Fig. 3B and C). Three-dimensional deconvolution was performed to confirm the locations of metastatic cells relative to the brain capillaries (Fig. 3D). One week after intracardiac injection, the brains of mice injected with normal BrLuc cells contained 3,331 ± 263 cells/brain (~1.9% of total cells injected), whereas brains of mice injected with TGFβ knockdown cells contained 1079 ± 495 cells/brain (~0.62% of total cells injected; Fig. 3E); this was a 68% reduction ($P < 0.001$) of cells in brain after knocking down TGFβ. The brains of mice treated with galunisertib

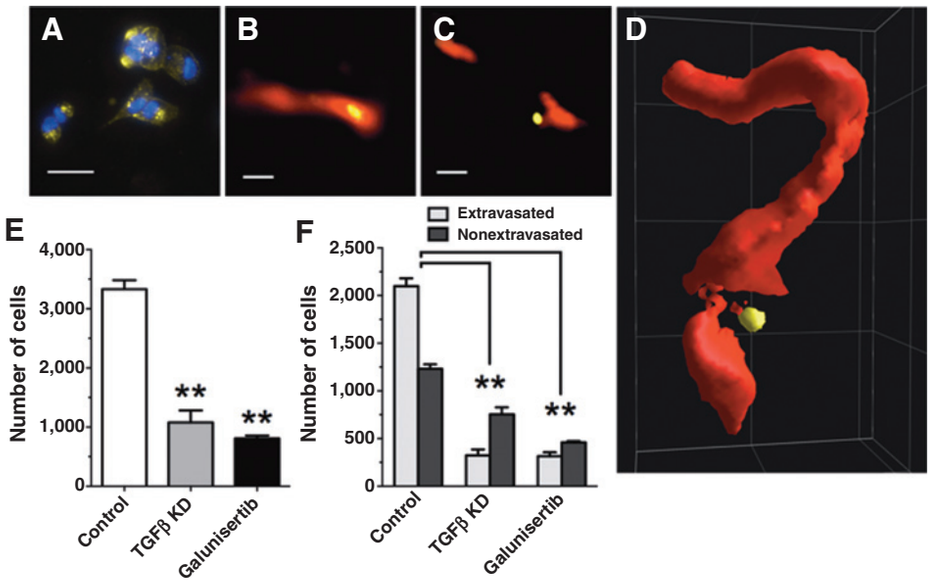

Figure 3.
TGFβ knockdown or receptor inhibition reduces seeding and extravasation of metastatic cells. All cells injected were labeled with quantum dots, cells were imaged to confirm efficient loading of quantum dots (A; DAPI-blue; yellow, metastatic cells with quantum dots). Immunofluorescence stained brain sections were stained against CD31 to label vasculature (red) to determine whether metastatic cells (yellow) remained within the lumen of the vasculature (B) or had extravasated the vessel (C). Three-dimensional fluorescence imaging combined with image 3-D deconvolution (constrained iterative algorithm) was performed to confirm quantum dot location in reference to CD31 stained vessels (D). The total number of cells detected in brain after one week (E). Ratios of extravasated and nonextravasated cells detected in each group (F; $n = 3$–5 for each group). All scale bars represent 10 μm. **, $P < 0.001$.

also had fewer ($P < 0.001$) metastatic cells (808 ± 82 cells/brain; Fig. 3E) leaving only 0.46% of the initial cells injected remaining after one week. The brains of mice injected with normal BrLuc cells had a larger percentage of cells that extravasated (63%) than cells remaining within the lumen of microvessels (37%; $P < 0.001$). There was a reduction in the percentage of cells that had extravasated from the TGFβ knockdown group (324 ± 106 cells; 30%) and galunisertib group (315 ± 70 cells; 40%) compared with the number of cells which had extravasated in the normal 231Br-Luc group (2,099 ± 140 cells; 63%; Fig. 3F). This resulted in a larger percentage of cells remaining confined within the vessel lumen of the brains of mice injected with TGFβ knockdown cells (755 ± 71 cells; 70%) and the galunisertib group (460 ± 23 cells; 60%) when compared with the number of cells which had remained in the vessel lumen in the normal 231Br-Luc group (1,232 ± 82; 37%). The ratios of the number of cells that extravasated beyond the vessel lumen for both the TGFβ-KD and galunisertib groups were reduced ($P < 0.001$) compared with control (Fig. 3F).

To determine whether this reduction in metastatic cells arresting and extravasating into brain would lead to a reduction in metastatic burden, randomized animals were sacrificed at predetermined times, brains were stained and analyzed for number and sizes of metastases. Animals that received normal 231Br-Luc cells did not begin to show detectable metastases until 21 days postinoculation (Fig. 4A). The greatest increase in the number of metastases in these animals occurred during the fourth week (~50-fold increase; no statistical test due to only $n = 2$ metastases detected from 5 mice on day 21); while there was no increase (day 28: 51.5 metastases; day 35: 45.3 metastases; $P > 0.79$) in metastases thereafter. Animals that received TGFβ knockdown cells displayed a delayed growth of metastases by one week (Fig. 4B). The earliest time-point which revealed metastasis growth was day 28 and the greatest increase in the number of metastases present occurred during the fifth week (days 28–35). There were fewer total metastases present in the brains of mice inoculated with TGFβ knockdown cells (5.5 ± 0.6 metastases on day 28, 13.5 ± 3.6 metastases on day 35; a ~90% and ~70% reduction, respectively, $P < 0.05$ for both). The size of metastatic lesions in the mice injected with normal 231Br-Luc cells increased the greatest (~3.4-fold) during the fourth week (0.17 ± 0.006 mm^2 on day 21, 0.56 ± 0.05 mm^2 for day 28; Fig. 4C). During the final week of the study, metastases continued to increase in size (1.3-fold) from the previous week. Mice bearing TGFβ knockdown cells showed a delayed growth (became detectable on day 28, ~ one week delay compared with the normal 231Br-Luc group; Fig. 4D); the greatest period of metastatic development took place between days 28 and 35 (2.45-fold increase in number of metastases). The average metastasis size in brains of mice inoculated with TGFβ knockdown cells grew from 0.079 ± 0.02 mm^2 on day 28 to 0.34 ± 0.05 mm^2 on day 35 (a ~4.3-fold increase in size between day 28 and day 35; $P < 0.001$), which followed a similar, but delayed trend of metastasis growth compared with animals injected with normal 231Br-Luc cells.

To determine whether the reduction of TGFβ would improve survival, a separate group of animals were injected with 231Br-Luc or 231Br-Luc-TGFβ knockdown cells. Animals injected with 231Br-Luc-TGFβ knockdown (median survival = 65 days; $n = 13$) survived longer (29 days longer; $P < 0.0001$; log-rank test) than animals injected with normal 231Br-Luc (median survival = 36 days; $n = 22$; Fig. 5).

Discussion

The only available treatments for breast cancer brain metastasis in the clinic remain restricted to chemotherapeutics, radiation, and surgery (24). In a majority of women with brain metastasis, chemotherapeutic strategies are utilized as the last line of treatment and often function only as palliative support (25). Unfortunately, restricted chemotherapeutic distribution to brain tumors and metastases is highly restricted because of the presence of the BBB, which continues to be the major obstacle to the successful treatment of brain metastases (26). In our experimental brain metastases of breast cancer model, we previously reported

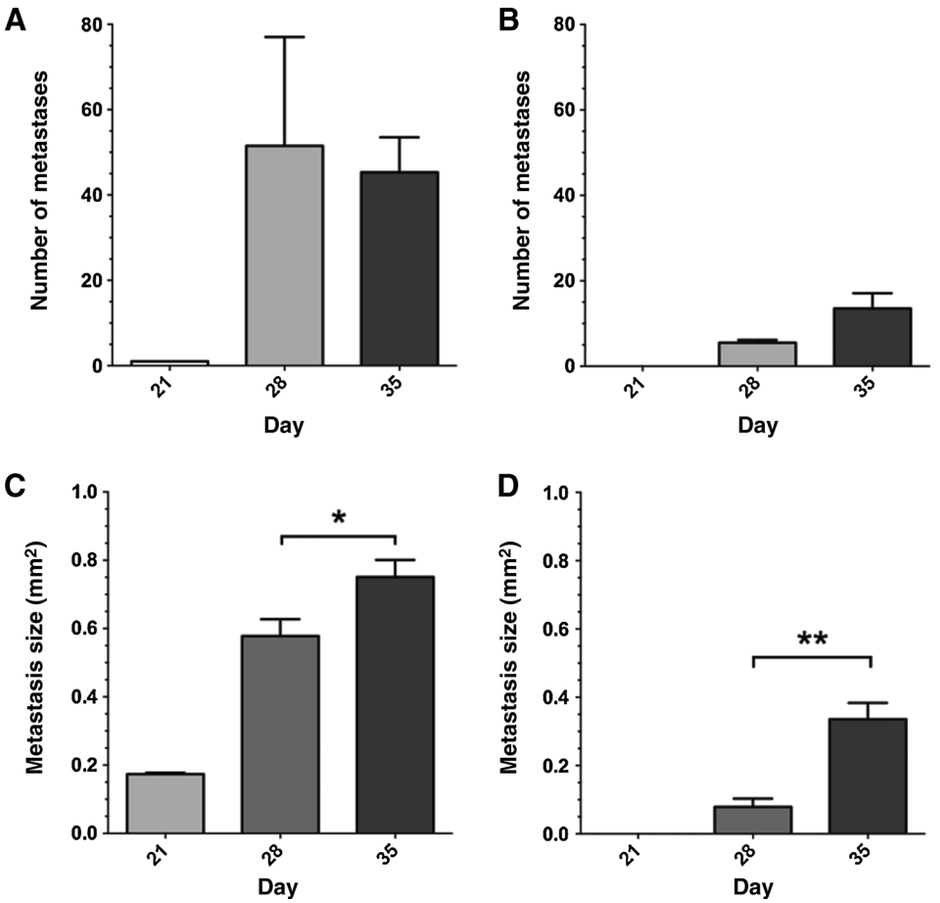

Figure 4.
TGFβ knockdown results in fewer and smaller metastases. The total number of detectable brain metastases of TNBC (A) and 231Br-Luc TGFβ knockdown (B) over time. The size (mm^2) of metastases for TNBC (C) and 231Br-Luc TGFβ knockdown group (D) over time ($n = 3$–5 for each time point for each group). *, $P < 0.05$; **, $P < 0.001$.

that high-HER2 breast cancer cells (MDA-MB-231Br-HH2) injected into anesthetized mice developed numerous brain metastases which exhibited variable permeability to paclitaxel and predicted that about 10% of brain metastases had permeability values sufficient to permit efficacious concentrations of chemotherapeutics (27). These observations may partly explain the variable responses to chemotherapy seen in the clinic (28–30). It is, therefore, our opinion that the prevention of brain metastases of breast cancer remains an under-studied research area to alleviate this disease. Until recently, metastatic prevention techniques used to modify therapeutic and preclinical outcomes about secondary brain metastasis have lacked sufficient and adequate methods to study individual steps of the metastatic process.

The study herein utilizes novel brain-seeking breast cancer sublines (231-Br), which were isolated by repeated cycles of intracardiac injection, harvesting of brain metastases, and *ex vivo* culture (21, 31). These brain-seeking metastatic cells are injected into the left cardiac ventricle, circulate in the peripheral vasculature, arrest in brain capillaries ("seed"), extravasate across the *in vivo* BBB, and finally develop a metastatic lesion. After neurologic symptoms develop, permeability studies are completed. When 231Br brain contrast-enhancing metastases (32) in mice were compared with a cohort of 16 resected human brain metastases of breast cancer, equivalent rates of proliferation, apoptosis, and neuro-inflammatory response were noted in both, thus supporting model relevance to human disease (33).

Recent clinical data suggest that removal of a primary breast tumor results in increased circulating tumor cells (CTC) in blood (34–37). The data show in approximately 4% to 22% of patients with primary tumor removal have increased CTCs (same phenotype as the primary tumor), which persist for 2 to 4 weeks (35–37). Importantly, retrospective analyses demonstrate that mastectomies increase the time to metastasis-related mortality, in a subset of women, by more than one year compared with women without tumor removal (34, 38). Tumor removal is suggested to accelerate the metastatic process (38). Injecting approximately 175 k brain-seeking cells into the circulation may reflect increases in CTCs after tumor perturbation. Importantly, vascular concentration of cells after our injection is within cell concentrations shed into the circulation every hour (98–206 k/cells/hour) by tumors in metastatic preclinical models and in humans (39–44). Our data may have direct translational application in reducing the effect of increased CTCs for an approximately 30-day window after surgical intervention. Increased numbers of CTCs are strongly correlated with poor outcomes associated with metastatic breast cancer (45, 46).

A number of studies have utilized knockdown and pharmacologic techniques to inhibit metastasis dependent pathways; however, these previous studies determined end time point results and lack quantitative information about specific steps of metastasis. For instance, Zhang and colleagues demonstrated the overall reduction and increased survival in a mouse melanoma metastasis

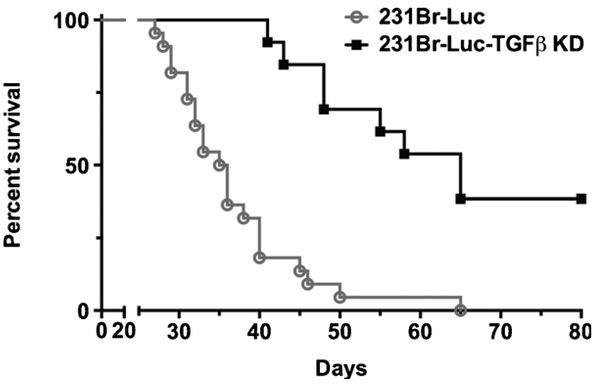

Figure 5.
TGFβ knockdown results in an extension of survival. TGFβ expression knockdown increases survival. The resulting Kaplan–Meier survival plot for both normal 231-Br (grey) and the 231-Br-TGFβ-KD (black) groups. The MDA-MB-231Br group ($n = 22$) had a mean survival of 36 days, whereas the 231Br-TGFβ-KD group ($n = 13$) had a mean survival of 62 days ($P < 0.0001$).

model by knocking down TGFβ (17). This study provides valuable data about the potential use of targeting TGFβ and its downstream pathway to enhance survival, but it does not evaluate and quantitate important steps such as tumor cell extravasation at the BBB and entry into brain. Therefore, there exists the need to expand and improve upon existing models and methods to evaluate the efficacy of potential pharmacologic agents seeking to hinder specific steps of the metastatic process.

To develop a detailed assay to investigate important steps involved in the metastatic process at the BBB, we chose to modulate TGFβ in our breast cancer metastasis model. TGFβ is strongly involved in the epithelial-to-mesenchymal transition and its downstream signaling involves the activation of SMAD transcription factors which regulate many genes associated with proliferation, differentiation, and migration (47).

By disturbing TGFβ signaling in our metastasis model, both by TGFβ receptor inhibition using galunisertib (48, 49) and shRNA-mediated TGFβ knockdown, we were able to specifically and quantitatively evaluate a role TGFβ plays in affecting cellular arrest within capillaries and their successive ability to extravasate beyond the brain capillary lumen and gain access to parenchyma. The process of extravasation is critical for the successful colonization of metastasis in the CNS; moreover, the postextravasation growth stage is proposed as the rate-limiting step of the metastatic process (50). Our method is able to quantitate this phase and provide relatively rapid feedback about biologic or pharmacologic manipulation aiming to disrupt one or more pathways integrated into the metastatic phenotype. To our knowledge, few other assays are collectively capable of providing data which we describe herein. The majority of BBB extravasation studies have been contributed by studies focusing on inflammation and the associated invasion of cells of the immune system during inflammation and injury within brain (51–53). One such assay developed to study T-cell transmigration across an *in vitro* BBB model provides the capability to quantitate the amount of rolling or capture of activated T-cells and their subsequent crawling and diapedesis (15). Although the mechanisms utilized by cells of the immune system are likely to be fairly similar to those necessary for tumor cell extravasation, due to the structural, behavioral, and molecular differences between immune cells and CTCs, their exact mechanism to cross the BBB may be very different (54). Many *in vivo* metastases studies have relied on longitudinal MRI studies relying on iron-loaded metastatic cells (18); however, MRI-based imaging modalities lack the resolution necessary to distinguish intravascular versus extravasated metastatic cells. Recently, Kienast and colleagues (55) reported a novel longitudinal *in vivo* imaging method to study metastatic cells and their individual fate in brain; these new *in vivo* imaging modalities coupled with relevant preclinical models will provide powerful tools for future brain metastasis research. Because we were able to show reductions in tumor cell arrest and extravasation across the BBB after TGFβ modulation, by pharmacologic inhibition or expression knockdown, translated to fewer metastasis development and increased overall survival, this technique provides a method to evaluate a drugs ability to prevent not only breast metastases to brain, but also of other primary malignancies and their subsequent metastasis to distant sites.

In conclusion, we detail a novel method to evaluate and quantitate critical steps needed for successful metastasis colonization. This will provide researchers with invaluable data reflecting the biologic process or pharmacologic response during metastasis and should expedite the development of treatments aimed at preventing metastases in women at risk for metastasis. With the increasing trend of brain metastases of breast cancer, especially in younger women, the successful development of treatments preventing this disease is in great demand.

Disclosure of Potential Conflicts of Interest

No potential conflicts of interest were disclosed.

Authors' Contributions

Conception and design: C.E. Adkins, R.K. Mittapalli, P.R. Lockman
Development of methodology: C.E. Adkins, M.I. Nounou, R.K. Mittapalli, P.R. Lockman
Acquisition of data (provided animals, acquired and managed patients, provided facilities, etc.): C.E. Adkins, M.I. Nounou, T.B. Terrell-Hall, A.S. Mohammad
Analysis and interpretation of data (e.g., statistical analysis, biostatistics, computational analysis): C.E. Adkins, M.I. Nounou, A.S. Mohammad, R. Jagannathan, P.R. Lockman
Writing, review, and/or revision of the manuscript: C.E. Adkins, R.K. Mittapalli, T.B. Terrell-Hall, A.S. Mohammad, P.R. Lockman
Administrative, technical, or material support (i.e., reporting or organizing data, constructing databases): C.E. Adkins
Study supervision: M.I. Nounou, P.R. Lockman
Other (involved in analysis of data; editing, and critically revising the manuscript): R. Jagannathan

Grant Support

This work was supported by a grant from the National Cancer Institute (R01CA166067-01A1), and a Department of Defense Breast Cancer Research Program grant (W81XWH-062-0033) awarded to PL. Additional support for this research was provided by WVCTSI through the National Institute Of General Medical Sciences of the National Institutes of Health under Award Number U54GM104942. A portion of this work was completed at each institution mentioned in the author affiliations.

The costs of publication of this article were defrayed in part by the payment of page charges. This article must therefore be hereby marked *advertisement* in accordance with 18 U.S.C. Section 1734 solely to indicate this fact.

Received July 14, 2014; revised September 23, 2014; accepted October 14, 2014; published OnlineFirst October 27, 2014.

References

1. Johnson RH, Chien FL, Bleyer A. Incidence of breast cancer with distant involvement among women in the United States, 1976 to 2009. JAMA 2013;309:800–5.
2. Smid M, Wang Y, Zhang Y, Sieuwerts AM, Yu J, Klijn JG, et al. Subtypes of breast cancer show preferential site of relapse. Cancer Res 2008;68: 3108–14.
3. Shaffrey ME, Mut M, Asher AL, Burri SH, Chahlavi A, Chang SM, et al. Brain metastases. Curr Probl Surg 2004;41:665–741.
4. Engel J, Eckel R, Aydemir U, Aydemir S, Kerr J, Schlesinger-Raab A, et al. Determinants and prognoses of locoregional and distant progression in breast cancer. Int J Radiat Oncol Biol Phys 2003;55:1186–95.
5. Lin NU, Bellon JR, Winer EP. CNS metastases in breast cancer. J Clin Oncol 2004;22:3608–17.
6. Bent vd. The role of chemotherapy in brain metastases. Eur J Cancer 2003;39:2114–20.
7. Lin N, Carey L, Liu M, Younger J, Come S, Ewend M, et al. Phase II trial of lapatinib for brain metasetases in patients with human epidermal growth factor receptor 2-positive breast cancer. Clin Cancer Res 2008;26:1993–9.
8. Ekenel M, Hormigo A, Peak S, DeAngelis L, Abrey L. Capecitabine therapy of central nervous system metastases from breast cancer. J Neurooncol 2007;85:223–7.
9. Rivera E, Meyers C, Groves M, Valero V, Francis D, Arun B, et al. Phase I study of capecitabine in combination with temozolomide in the treatment of patients with brain metastases of breast cancer. Cancer 2006;107: 1348–54.
10. Lipinski CA, Lombardo F, Dominy BW, Feeney PJ. Experimental and computational approaches to estimate solubility and permeability in drug discovery and development settings. Adv Drug Deliv Rev 2001;46:3–26.
11. Genka S, Deutsch J, Shetty UH, Stahle PL, John V, Lieberburg IM, et al. Development of lipophilic anticancer agents for the treatment of brain tumors by the esterification of water-soluble chlorambucil. Clin Exp Metastasis 1993;11:131–40.
12. Lesser GJ, Grossman SA, Eller S, Rowinsky EK. The distribution of systemically administered [3H]-paclitaxel in rats: a quantitative autoradiographic study. Cancer Chemother Pharmacol 1995;37:173–8.
13. Rowinsky EK. On pushing the outer edge of the outer edge of paclitaxel's dosing envelope. Clin Cancer Res 1999;5:481–6.
14. Zimmermann M, Box C, Eccles SA. Two-dimensional vs. three-dimensional *in vitro* tumor migration and invasion assays. Methods Mol Biol 2013;986:227–52.
15. Coisne C, Lyck R, Engelhardt B. Live cell imaging techniques to study T cell trafficking across the blood-brain barrier *in vitro* and *in vivo*. Fluids Barriers CNS 2013;10:7.
16. Lippmann ES, Al-Ahmad A, Palecek SP, Shusta EV. Modeling the blood-brain barrier using stem cell sources. Fluids Barriers CNS 2013;10:2.
17. Zhang C, Zhang F, Tsan R, Fidler IJ. Transforming growth factor-beta2 is a molecular determinant for site-specific melanoma metastasis in the brain. Cancer Res 2009;69:828–35.
18. Heyn C, Ronald JA, Ramadan SS, Snir JA, Barry AM, MacKenzie LT, et al. *In vivo* MRI of cancer cell fate at the single-cell level in a mouse model of breast cancer metastasis to the brain. Magn Reson Med 2006;56:1001–10.
19. Marsden CG, Wright MJ, Carrier L, Moroz K, Pochampally R, Rowan BG. A novel *in vivo* model for the study of human breast cancer metastasis using primary breast tumor-initiating cells from patient biopsies. BMC Cancer 2012;12:10.
20. Palmieri D, Chambers AF, Felding-Habermann B, Huang S, Steeg PS. The biology of metastasis to a sanctuary site. Clin Cancer Res 2007;13: 1656–62.
21. Yoneda T, Williams P, Hiraga T, Niewolna M, Nishimura R. A bone seeking clone exhibits different biological properties from the MDA-MB-231 parental human breast cancer cells and a brain-seeking clone *in vivo* and *in vitro*. J Bone and Mineral Res 2001;16:1486–95.
22. Kappes JC, Wu X. Safety considerations in vector development. Magn Reson Med 2001;26:147–58.
23. Kappes JC, Wu X, Wakefield JK. Production of trans-lentiviral vector with predictable safety. Methods Mol Med 2003;76:449–65.
24. Cheng X, Hung MC. Breast cancer brain metastases. Cancer Metastasis Rev 2007;26:635–43.
25. Steeg PS, Camphausen KA, Smith QR. Brain metastases as preventive and therapeutic targets. Nat Rev Cancer 2011;11:352–63.
26. Motl S, Zhuang Y, Waters CM, Stewart CF. Pharmacokinetic considerations in the treatment of CNS tumors. Clin Pharmacokinet 2006;45: 871–903.
27. Lockman PR, Mittapalli RK, Taskar KS, Rudraraju V, Gril B, Bohn KA, et al. Heterogeneous blood-tumor barrier permeability determines drug efficacy in experimental brain metastases of breast cancer. Clin Cancer Res 2010; 16:5664–78.
28. Boogerd W, Dalesio O, Bais EM, van der Sande JJ. Response of brain metastases from breast cancer to systemic chemotherapy. Cancer 1992; 69:972–80.
29. Freilich RJ, Seidman AD, DeAngelis LM. Central nervous system progression of metastatic breast cancer in patients treated with paclitaxel. Cancer 1995;76:232–6.
30. Abrey LE, Olson JD, Raizer JJ, Mack M, Rodavitch A, Boutros DY, et al. A phase II trial of temozolomide for patients with recurrent or progressive brain metastases. J Neurooncol 2001;53:259–65.
31. Palmieri D, Bronder JL, Herring JM, Yoneda T, Weil RJ, Stark AM, et al. Her-2 overexpression increases the metastatic outgrowth of breast cancer cells in the brain. Cancer Res 2007;67:4190–8.
32. Song HT, Jordan EK, Lewis BK, Liu W, Ganjei J, Klaunberg B, et al. Rat model of metastatic breast cancer monitored by MRI at 3 tesla and bioluminescence imaging with histological correlation. J Transl Med 2009;7:88.
33. Fitzgerald D, Palmieri D, Hua E, Hargrave E, Herring J, Qian Y, et al. Reactive glia are recruited by highly proliferative brain metastases of breast cancer and promote tumor cell colonization. Clin Exp Metast 2008; 25:799–810.
34. Biggers B, Knox S, Grant M, Kuhn J, Nemunaitis J, Fisher T, et al. Circulating tumor cells in patients undergoing surgery for primary breast cancer: preliminary results of a pilot study. Ann Surg Oncol 2009;16:969–71.
35. Sandri MT, Zorzino L, Cassatella MC, Bassi F, Luini A, Casadio C, et al. Changes in circulating tumor cell detection in patients with localized breast cancer before and after surgery. Ann Surg Oncol 2010;17: 1539–45.
36. Krag DN, Ashikaga T, Moss TJ, Kusminsky RE, Feldman S, Carp NZ, et al. Breast cancer cells in the blood: a pilot study. Breast J 1999;5:354–8.
37. Banys M, Krawczyk N, Becker S, Jakubowska J, Staebler A, Wallwiener D, et al. The influence of removal of primary tumor on incidence and phenotype of circulating tumor cells in primary breast cancer. Breast Cancer Res Treat 2012;132:121–9.
38. Demicheli R, Valagussa P, Bonadonna G. Does surgery modify growth kinetics of breast cancer micrometastases? Br J Cancer 2001;85:490–2.
39. Danila DC, Heller G, Gignac GA, Gonzalez-Espinoza R, Anand A, Tanaka E, et al. Circulating tumor cell number and prognosis in progressive castration-resistant prostate cancer. Clin Cancer Res 2007;13:7053–8.
40. Hayashi K, Jiang P, Yamauchi K, Yamamoto N, Tsuchiya H, Tomita K, et al. Real-time imaging of tumor-cell shedding and trafficking in lymphatic channels. Cancer Res 2007;67:8223–8.
41. Glaves D. Correlation between circulating cancer cells and incidence of metastases. Br J Cancer 1983;48:665–73.
42. Swartz MA, Kristensen CA, Melder RJ, Roberge S, Calautti E, Fukumura D, et al. Cells shed from tumors show reduced clonogenicity, resistance to apoptosis, and *in vivo* tumorigenicity. Br J Cancer 1999;81:756–9.
43. Liotta LA, Kleinerman J, Saidel GM. Quantitative relationships of intravascular tumor cells, tumor vessels, and pulmonary metastases following tumor implantation. Cancer Res 1974;34:997–1004.
44. Butler TP, Gullino PM. Quantitation of cell shedding into efferent blood of mammary adenocarcinoma. Cancer Res 1975;35:512–6.
45. Zhao S, Liu Y, Zhang Q, Li H, Zhang M, Ma W, et al. The prognostic role of circulating tumor cells (CTCs) detected by RT-PCR in breast cancer: a meta-analysis of published literature. Breast Cancer Res Treat 2011;130: 809–16.
46. Janni W, Vogl FD, Wiedswang G, Synnestvedt M, Fehm T, Juckstock J, et al. Persistence of disseminated tumor cells in the bone marrow of breast cancer patients predicts increased risk for relapse–a European pooled analysis. Clin Cancer Res 2011;17:2967–76.
47. Derynck R, Akhurst RJ, Balmain A. TGF-beta signaling in tumor suppression and cancer progression. Nat Genet 2001;29:117–29.
48. Liu Z, Kobayashi K, van Dinther M, van Heiningen SH, Valdimarsdottir G, van Laar T, et al. VEGF and inhibitors of TGFbeta type-I receptor kinase

synergistically promote blood-vessel formation by inducing alpha5-integrin expression. J Cell Sci 2009;122:3294–302.
49. Bueno L, de Alwis DP, Pitou C, Yingling J, Lahn M, Glatt S, et al. Semi-mechanistic modeling of the tumor growth inhibitory effects of LY2157299, a new type I receptor TGF-beta kinase antagonist, in mice. Eur J Cancer 2008;44:142–50.
50. Chambers AF, MacDonald IC, Schmidt EE, Koop S, Morris VL, Khokha R, et al. Steps in tumor metastasis: new concepts from intravital videomicroscopy. Cancer Metastasis Rev 1995;14:279–301.
51. Lyck R, Engelhardt B. Going against the tide–how encephalitogenic T cells breach the blood-brain barrier. J Vasc Res 2012;49:497–509.
52. Cucullo L, Marchi N, Hossain M, Janigro D. A dynamic *in vitro* BBB model for the study of immune cell trafficking into the central nervous system. J Cereb Blood Flow Metab 2011;31:767–77.
53. Reijerkerk A, Lakeman KA, Drexhage JA, van Het Hof B, van Wijck Y, van der Pol SM, et al. Brain endothelial barrier passage by monocytes is controlled by the endothelin system. J Neurochem 2012;121:730–7.
54. Strell C, Entschladen F. Extravasation of leukocytes in comparison to tumor cells. Cell Commun Signaling 2008;6:10.
55. Kienast Y, von Baumgarten L, Fuhrmann M, Klinkert WE, Goldbrunner R, Herms J, et al. Real-time imaging reveals the single steps of brain metastasis formation. Nat Med 2010;16:116–22.